Atomic oxygen adsorption and incipient oxidation of the Pb(111) surface: A density-functional theory study

Bo Sun,[1] Ping Zhang,[1,2,*] Zhigang Wang,[1] Suqing Duan,[1] Xian-Geng Zhao,[1] Xucun Ma,[3] and Qi-Kun Xue[3]
[1]*LCP, Institute of Applied Physics and Computational Mathematics, P.O. Box 8009, Beijing 100088, People's Republic of China*
[2]*Center for Applied Physics and Technology, Peking University, Beijing 100871, People's Republic of China*
[3]*Institute of Physics, Chinese Academy of Sciences, Beijing 100080, People's Republic of China*
(Received 18 August 2007; revised manuscript received 7 June 2008; published 11 July 2008)

We study the atomic oxygen adsorption on Pb(111) surface by using density-functional theory within the generalized gradient approximation and a supercell approach. The atomic and energetic properties of purely on-surface and subsurface oxygen structures at the Pb(111) surface are systematically investigated for a wide range of coverage and adsorption sites. The fcc and tetra-II sites (see the text for definition) are found to be energetically preferred for the on-surface and subsurface adsorption, respectively, in the whole range of coverage considered. The on-surface and subsurface oxygen binding energies monotonically increase with the coverage, and the latter is always higher than the former, thus indicating a tendency to the formation of oxygen islands (clusters) and the higher stability of subsurface adsorption. The on-surface and subsurface diffusion-path energetics of atomic oxygen, as well as the activation barriers for oxygen penetration from the on-surface to the subsurface sites, are presented at low and high coverage. The other properties of the O/Pb(111) system, including the charge distribution, the lattice relaxation, the work function, and the electronic density of states, are also studied and discussed in detail. It is pointed out that the O-Pb chemical bonding during surface oxidation displays a mixed ionic/covalent character. Here the ionicity is featured by a charge flow from Pb $6p$ to O $2p$ states, while the covalency is featured by the Pb $6s^2$ "lone pair" effect, which results from hybridization of Pb $6s$ and O $2p$ states.

DOI: 10.1103/PhysRevB.78.035421 PACS number(s): 68.43.Bc, 68.43.Fg, 68.43.Jk, 73.20.Hb

I. INTRODUCTION

Lead (Pb) is one kind of heavy metal element with widespread availability. Single crystal Pb is extremely resistant to oxygen.[1] Appreciable oxidation takes place only at relatively high temperature ($\geq$370 K) or at considerable oxygen coverage at room temperature. However, this inoxidability of lead can be overcome by a so-called two-step treatment:[2] (i) low-temperature (100 K) adsorption, followed by (ii) annealing at elevated temperatures to above 220 K. The method itself proves to be a very effective way for low-temperature surface oxidation. Using this two-step approach, recently the oxygen adsorption on ultrathin Pb(111) films was experimentally investigated by using the scanning tunneling microscopy (STM) and scanning tunneling spectroscopy (STS) measurements.[3] Remarkably, it was found that the surface oxidation displays a prominent quantum oscillating effect by varying the thickness of Pb(111) film. Furthermore, it was found that the O adsorbates can form some magic clusters with regular size and shape.[4] These phenomena of oxygen adsorption and surface oxidation at Pb(111) remain yet to be exploited and understood, which is a main driving force for our present first-principles study. Contrary to the extensive first-principles studies of the surface oxidation on transition metals (TMs) such as Cu,[5–13] Ag,[14–25] Rh,[26–29] Pd,[30–34] Pt,[35–39] and Ru,[40,41] and on the simple *sp* metals such as Al (Refs. 42–48) and Mg,[49–51] *ab initio* studies of oxygen chemisorption on Pb(111) surface, in particular, O subsurface species on Pb(111) surface, are still lacking.

In this paper, we have carried out the first-principles calculations of on-surface and subsurface oxygen adsorption at Pb(111) in a wide range of coverage. Results for the determination of stable adsorption sites, work-function and atomic-relaxation changes, charge densities, electronic structures, and energy barriers for O diffusion and penetration, are systematically presented. Like other metals, surface oxidation of Pb is expected to involve three main events: (i) The initial dissociation of O_2 molecules and oxygen chemisorption on Pb(111) surface, followed by (ii) lattice penetration of atomic oxygen and oxide nucleation, and finally (iii) crystallization and growth of the stoichiometric oxide phases. The sequence of these events may be complex, and rather than successively, they may occur simultaneously, depending on temperature and pressure. The main purpose of this paper is to give a partial but definite understanding of events (i) and (ii) by studying the energetics and structures of atomic O adsorbates with purely on-surface and subsurface adsorption sites and with different coverage. A full study involving the initial dissociation of O_2 molecules when approaching to or accumulating on the Pb(111) surface, and the penetration process, which involves simultaneous on-surface and subsurface adsorption, will be given elsewhere. In particular, since the atomic oxygen adsorption and diffusion on metal surface are elementary processes toward the whole surface oxidation, and the atomic configuration after oxygen chemisorption may give a reasonable anticipation for the tendency of surface oxidation, it is expected that the present systematic first-principles calculations of oxygen adsorption on Pb(111) is of high interest in relation to understanding the nature of the O-Pb chemical bonding.

This paper is organized as follows. In Sec. II we give details of the first-principles total energy calculations, which is followed in Sec. III by our results for bulk Pb, the clean Pb(111) surface, and the O_2 molecule. The results for purely

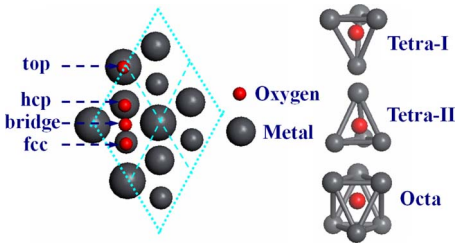

FIG. 1. (Color online) (Left panel) four on-surface adsorption sites including fcc, hcp, bridge (B2), and on-top (T1) sites. Note that Pb atoms of outmost three layers are shown by scaled gray balls (the larger ones are outer Pb atoms). (Right panel) three subsurface adsorption sites including tetra-I, tetra-II, and octa sites.

on-surface adsorption as a function of the oxygen coverage are presented in Sec. IV, where the surface and adsorption energetics, the atomic geometry, and the electronic structures are presented and analyzed. In Sec. V, we discuss the purely subsurface adsorption of oxygen atoms as we did in Sec. IV. The energy barriers for atomic oxygen diffusion and penetration are presented in Sec. VI, and the conclusion is given in Sec. VII.

II. CALCULATION METHOD

The density-functional theory (DFT) total energy calculations were carried out using the VIENNA *ab initio* simulation package[52] with the projector-augmented-wave (PAW) pseudopotentials[53] and plane waves.[54] In the present film calculations, the so-called *repeated slab* geometries were employed.[55] This scheme consists of the construction of a unit cell of an arbitrarily fixed number of atomic layers identical to that of the bulk in the plane of the surface (defining the bidimensional cell), but symmetrically terminated by an arbitrarily fixed number of empty layers (the "vacuum") along the direction perpendicular to the surface. In the present study, the clean Pb(111) surface is modeled by periodic slabs consisting of ten lead layers separated by a vacuum of 20 Å, which is found to be sufficiently convergent.[56] The oxygen atoms are adsorbed on both sides of the slab in a symmetric way. During our calculations, the positions of the outmost three lead layers, as well as the O atoms, are allowed to relax while the central four layers of the slab are fixed in their calculated bulk positions. The plane-wave energy cutoff was set 400 eV. If not mentioned differently we have used a $(12\times12\times1)$ k-point grid for the $p(1\times1)$ surface cell, $(6\times6\times1)$ k-point grid for the $p(\sqrt{3}\times\sqrt{3})$ and $p(2\times2)$ cells, and $(4\times4\times1)$ k-point grid for the $p(3\times3)$ cell, with Monkhorse-Pack scheme.[57] Furthermore, the generalized gradient approximation (GGA) of Perdew *et al.*[58] for the exchange-correlation potential was employed. A Fermi broadening[59] of 0.05 eV was chosen to smear the occupation of the bands around E_F by a finite-T Fermi function and extrapolating to $T=0$ K.

In the present paper, the calculations for oxygen atoms in the five adsorption sites, including on-surface (hcp and fcc) and subsurface (tetra-I, tetra-II, and octa) sites depicted in Fig. 1, have been performed for coverage ranging from 0.11 ML to a full monolayer. Specially, the oxygen coverages of 0.11 ML, 0.33 ML, and 0.67 ML were calculated using $p(3\times3)$ surface unit cell, while the coverage of 0.25 ML, 0.50 ML, 0.75 ML, and 1.0 ML were calculated in the $p(2\times2)$ surface cell containing one, two, three, and four oxygen atoms, respectively. The on-surface top (T1) and bridge (B2) adsorption sites were also considered. The T1 site was found to be notably less favorable than the fcc and hcp sites. When the O atom is placed on the B2 site, it always moves to the fcc site after relaxation. Actually, Fig. 15 will show that the B2 site is a saddle point in the O diffusion path from hcp to fcc site. Thus in this paper, most of the on-surface adsorption studies are focused on the fcc and hcp sites.

One central quantity tailored for the present study is the average binding energy of the adsorbed oxygen atom defined as

$$E_b(\Theta) = -\frac{1}{N_O}[E_{O/Pb(111)} - E_{Pb(111)} - N_O E_O], \qquad (1)$$

where N_O is the total number of O adatoms present in the supercell at the considered coverage Θ (we define Θ as the ratio of the number of adsorbed atoms to the number of atoms in an ideal substrate layer). $E_{O/Pb(111)}$, $E_{Pb(111)}$, and E_O are the total energies of the slabs containing oxygen, of the corresponding clean Pb(111) slab, and of a free O atom, respectively. According to this definition, E_b is also the adsorption energy E_{ad} per O atom, i.e., the energy that a free O atom gains upon its adsorption. Thus a positive value of E_b indicates that the adsorption is exothermic (stable) with respect to a free O atom and a negative value indicates endothermic (unstable) reaction. On the other hand, since in most cases, the oxygen chemisorption process inevitably involves the dissociation of O_2 molecules, thus the adsorption energy per oxygen atom can alternatively be referenced to the energy which the O atom has in the O_2 molecule by subtracting half the dissociation energy D of the O_2 molecule,

$$E_{ad(1/2O_2)} = E_b - D/2. \qquad (2)$$

With this choice of adsorption energy, then a positive value indicates that the dissociative adsorption of O_2 is an exothermic process, while a negative value indicates that it is endothermic and that it is energetically more favorable for oxygen to be in the gas phase as O_2.

III. BULK Pb, CLEAN Pb(111) SURFACE, AND OXYGEN MOLECULE

First, the total energy of the bulk fcc Pb was calculated to obtain the bulk lattice constant. The calculated lattice constant is $a=5.028$ Å, well comparable to the experimental value of 4.95 Å.[60] The 6s and 6p electrons of Pb atoms were treated as valence electrons and the 5d electrons were treated as core electrons. This choice of valence and core electrons has been previously employed to study the electronic properties of lead oxide [including PbO (Ref. 61) and PbO_2 (Ref. 62)]. Note that we have also studied the effect of Pb 5d electrons on the properties of clean and oxygen-adsorbed

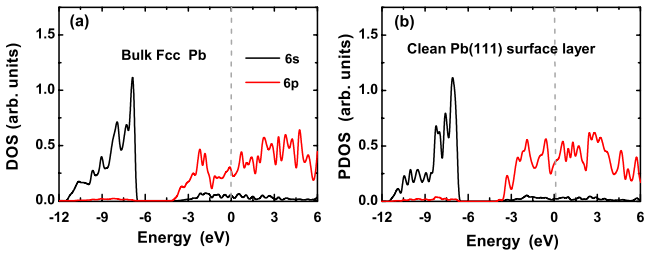

FIG. 2. (Color online) (a) Orbital-resolved DOS (per atom) for bulk Pb. (b) Orbital-resolved partial DOS for the clean 1×1 Pb(111) surface layer. The Fermi energy is indicated by the vertical dashed line at 0 eV.

Pb(111) surfaces and found no accountable changes by treating the Pb $5d$ electrons as valence electrons.[63] The orbital-resolved electronic density of states (DOS) per atom for the bulk Pb is shown in Fig. 2(a). The two broad peaks correspond to Pb $6s$ and $6p$ states. Compared to the $6s$ band, the $6p$ bands are more dispersive due to the extensive character of the atomic p orbitals. In addition, there is a small s-p hybridization near the Fermi energy.

The calculation for the atomic relaxations of the clean surface with $p(1\times1)$, $p(\sqrt{3}\times\sqrt{3})$, $p(2\times2)$, and $p(3\times3)$ periodicities (models) provides not only a test of the clean surface with different cell sizes, but is also used to evaluate the charge density difference used later and assess the changes in the work function by oxygen adsorption. Our clean-surface calculation shows that the two outmost Pb(111) layers relax significantly from the bulk values. The first-second interlayer contraction is nearly 5% and the second-third interlayer expansion is nearly 3%, which is in agreement with recent results from first-principles calculations[64,65] and the LEED experiment.[66] Note that the first interlayer separation on most metal surfaces is contracted compared to the bulk case; Pb(111) is also a typical example. The third-fourth interlayer relaxation is practically the same as the interlayer distance in the bulk. The variation of the work function is negligible for different surface cells [with a typical value of 3.83 eV, see the inset in Fig. 7(a)] and is in excellent agreement with other theoretical results.[64,65] The calculated charge density $n(\mathbf{r})$ (not depicted here) of the clean Pb(111) surface shows that similar to the other typical metal surfaces,[67] there is a rapid variation in $n(\mathbf{r})$ in the surface interstitial region, with $n(\mathbf{r})$ falling off sharply in magnitude toward the vacuum and soon "healing" the discrete atomic nature of the surface. This sizable charge redistribution near the surface is associated with the formation of the (uniform) surface dipole layer, which sensitively determines the work function.

As one knows, surface calculations are very subtle, requiring enough k-point mesh and efficient energy cutoff, the correct model, and the other details. To test the convergence of the physical properties of the clean Pb(111) surface, we have calculated and analyzed the interlayer relaxations $\Delta_{ij}=(d_{ij}-d_0)/d_0$ with respect to the bulk interlayer distance $d_0=2.903$ Å, the surface energy E_s, and the work function Φ of the clean Pb(111) slabs by using different models with various k-point meshes. The results are listed in Table I, from which it reveals that while the atomic interlayer relaxations are somewhat sensitive to the choice of k-point mesh and the supercells, the influences to the surface energetics from using different models are negligibly small. To keep the computation accuracy as high as possible for reliable comparison between different adsorption configurations, here we suggest calculating and analyzing surface energetics and electronic structures under the same model. For example, a $p(3\times3)$ surface unit cell is needed if one wants to analyze the properties of surface chemical activity in a coverage range beginning from $\Theta=0.11$.

Figure 2(b) plots the orbital-resolved site-projected density of states (PDOS) for the topmost Pb layer of the clean $p(1\times1)$ Pb(111) surface cell. Compared to Fig. 2(a), one can see that the surface electronic structure is almost the same as that of the bulk, with a little anisotropy in the $6p_{x,y}$ and $6p_z$ orbitals for the surface Pb atom. Note that throughout this paper we did not consider the quantum size effect on the atomic and electronic structures, since in our various supercell models the substrate has been fixed with the same thickness.

The total energies of the isolated O atom and free O_2 molecule are calculated in a cubic cell of side length 10 Å with a $(3\times3\times3)$ k-point mesh for the Brillouin zone sampling. The spin-polarization correction has been included. The binding energy of O_2 is calculated to be $1/2E_b^{O_2}=3.12$ eV per atom and the O-O bond length is about 1.235 Å. These results are typical for well-converged DFT-GGA calculations. Compared to the experimental[68] values of 2.56 eV and 1.21 Å for O binding energy and bonding length, the usual DFT-GGA result always introduces an overestimation, which reflects the theoretical deficiency for describing the local orbitals of the oxygen. The resultant error in calculating the absolute value of the binding energy, however, does not matter in this work, since it is the difference in

TABLE I. The calculated interlayer relaxation Δ_{ij} (%), surface energy E_s (in eV), and work function Φ (in eV) for different clean Pb(111) surface models with different k-point meshes.

Model	k-point mesh	irreducible k	Δ_{12} (%)	Δ_{23} (%)	Δ_{34} (%)	E_s (eV)	Φ (eV)
1×1	$12\times12\times1$	216	−4.670	2.560	−0.149	0.372	3.830
1×1	$6\times6\times1$	54	−5.326	3.066	−0.267	0.350	3.786
$\sqrt{3}\times\sqrt{3}$	$6\times6\times1$	54	−5.110	2.090	0.160	0.360	3.833
2×2	$6\times6\times1$	54	−4.803	2.977	−0.100	0.372	3.830
3×3	$4\times4\times1$	24	−4.882	2.890	0.369	0.373	3.832
3×3	$3\times3\times1$	5	−5.978	2.831	1.320	0.372	3.834

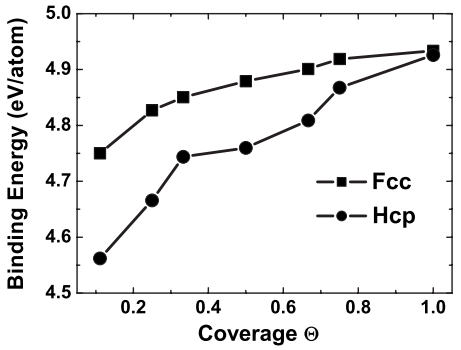

FIG. 3. Calculated binding energies of O/Pb(111) systems, with oxygen in the fcc (solid squares) and hcp (solid circles) sites, as functions of the oxygen coverage. The solid lines connecting the calculated binding energies are used to guide the eyes.

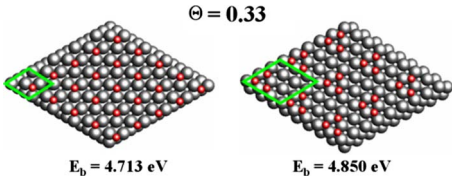

FIG. 4. (Color online) Two kinds of configurations for O_{fcc} adsorbates at the same coverage $\Theta=0.33$. The oxygen adatoms in the right panel are arranged to be clustered, while the left panel gives a uniform distribution. The calculated total energies show that the adsorption in the right panel is more stable.

binding energies of two geometries that determines which one is more stable (if they contain the same amount of oxygen atoms) or how E_b evolves with coverage (if the structures contain an unequal amount of oxygen atoms). We will consider this overbinding of O_2 when drawing any conclusion that may be affected by its explicit value.

IV. PURE ON-SURFACE ADSORPTION

For different oxygen coverage Θ, the binding energies E_b for oxygen adatom on fcc and hcp sites of Pb(111) surface, with respect to the free atomic oxygen, are illustrated in Fig. 3 and summarized in Table II. One can see from Fig. 3 that this quantity for both fcc and hcp adsorption displays a modestly increasing tendency with the oxygen coverage, while the overall variation in the magnitude of E_b is rather small in the range of coverage we considered. The increasing binding energy with coverage indicates a prominent attraction between the on-surface oxygen atoms and implies a tendency to form oxygen islands or clusters on the Pb(111) surface. This result is similar to that of the O-adsorbed Al(111) and Mg(0001) surfaces, compared to which the increase in E_b slows down with coverage in the present O/Pb(111) system. Note that in the oxygen/TM systems, the binding energy E_b decreases due to the increasing electron occupation of the antibonding states as a function of the oxygen coverage. On the other hand, considering the binding energy E_b of atomic oxygen on the surface with respect to the half of the binding energy for the O_2 molecule (the calculated value of 3.12 eV or experimental value of 2.56 eV), the present calculations predict that in the whole coverage range we considered, the atomic oxygen on-surface adsorption is stable. Also it reveals in Fig. 3 that the fcc site is energetically favorable relative to the hcp site, although their difference in E_b decreases with increasing Θ, namely, from 0.19 eV at $\Theta=0.11$ down to (less than) 0.01 eV at $\Theta=1.0$.

To further clarify our observation that the oxygen adsorbates tend to form clusters on the Pb(111) surface, here as one typical example, we consider two kinds of arrangements for O_{fcc} adsorbates at the same coverage $\Theta=0.33$. These two adsorbate arrangements are shown in Fig. 4. The left panel in Fig. 4 corresponds to the case of a $p(\sqrt{3}\times\sqrt{3})$ surface cell, while the right panel gives one selective adsorbate configuration produced from the $p(3\times3)$ surface cell. Obviously, the oxygen adatoms in the right panel are more clustered than those in the left panel. Remarkably, the calculated binding energy is $E_b=4.713$ eV for the left panel and $E_b=4.85$ eV for the right panel, which clearly shows the preference for the formation of oxygen clusters on the Pb(111) surface.

Table III presents the calculated results for the relaxed atomic structures, including the height $h_{O\text{-}Pb}$ of O above the surface, the O-Pb bond length R_1, and the interlayer relax-

TABLE II. The calculated binding energy E_b (in eV) and work function Φ (in eV) as functions of oxygen coverage for five on-surface and subsurface adsorption sites.

	Site	$\Theta=0.11$	0.25	0.33	0.5	0.67	0.75	1.0
E_b	fcc	4.750	4.827	4.850	4.879	4.901	4.919	4.934
	hcp	4.562	4.666	4.744	4.760	4.809	4.868	4.926
	tetra-I	4.771	4.785	4.863	4.887	4.920	5.019	5.139
	tetra-II	4.842	4.907	4.927	4.957	5.006	5.053	5.145
	octa	4.628	4.545	4.776	4.876	4.870	4.862	5.012
Φ	fcc	3.966	4.002	4.107	4.208	5.056	4.501	4.669
	hcp	3.941	3.953	4.085	4.205	4.998	4.367	4.599
	tetra-I	3.812	3.787	3.736	3.630	3.463	3.630	3.411
	tetra-II	3.809	3.776	3.721	3.680	3.383	3.510	3.214
	octa	3.807	3.775	3.716	3.567	3.420	3.504	3.342

TABLE III. The calculated atomic interlayer relaxation Δ_{ij} (%), O-Pb bond length R_1 (in Å), and the adsorbate height $h_{\text{O-Pb}}$ (in Å) for different oxygen coverage of on-surface adsorption.

	$h_{\text{O-Pb}}$ (Å)		R_1 (Å)		Δ_{12} (%)		Δ_{23} (%)	
Coverage	fcc	hcp	fcc	hcp	fcc	hcp	fcc	hcp
0.11	1.116	1.115	2.282	2.289	−3.098	−3.567	1.752	−0.492
0.25	0.914	0.876	2.266	2.268	−1.641	−0.413	1.378	−0.601
0.33	1.047	0.939	2.257	2.274	−1.568	−0.095	0.779	−0.176
0.50	0.975	1.010	2.265	2.269	3.405	4.562	−0.614	−2.498
0.75	0.980	0.944	2.258	2.252	12.995	12.298	−2.445	−3.243
1.00	0.971	0.970	2.271	2.272	20.363	21.002	−5.085	−4.863

ations Δ_{ij} for various coverage with O in the fcc and hcp sites. For more clear illustration, the first and second interlayer relaxations (Δ_{12} and Δ_{23}) are also plotted in Fig. 5 as functions of oxygen coverage. One can see that the adsorption of oxygen on Pb(111) induces notable changes in the interlayer distance of the substrate. In particular, the topmost interlayer relaxation (Δ_{12}) changes from contraction (about −5%) to expansion (about 20%), and on the contrary, the second interlayer relaxation (Δ_{23}) changes from expansion (about 3%) to contraction (about −5%), for O in both fcc and hcp sites. This large and sign-inverted change of atomic interlayer relaxations upon oxygen adsorption is unique for O/Pb(111) when comparing with other oxygen/metal systems. For instance, at Al(111) surface, the topmost interlayer relaxation on oxygen adsorption is at most Δ_{12}=4%,[47] while at Ag(111) surface, there is even no change of interlayer relaxations before and after oxygen adsorption. The large expansion in Pb(111) interlayer relaxations reflects the strong influence of the O adsorbate on the neighboring Pb atoms, and thus results from important redistribution of the electronic structure. Concerning the O-Pb bond length R_1 at different oxygen coverage, one can see from Table III that for both fcc and hcp adsorption, the O-Pb bond length varies around 2.26 Å very little with increasing Θ. In particular, the calculated results of R_1 by using the same $p(2\times2)$ surface model vary only within an amplitude of 0.01 Å (0.02 Å) for fcc (hcp) site. The short bond length R_1 implies a strong interaction between O and Pb atoms. Note that the value of R_1 for O_{fcc} is slightly shorter than that for O_{hcp}, which is consistent with the fact that the fcc site is more stable than the hcp site for on-surface adsorption.

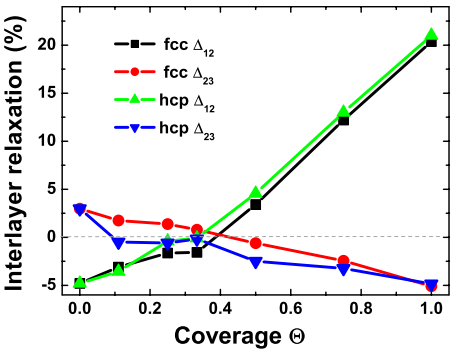

FIG. 5. (Color online) Atomic interlayer relaxations as functions of coverage for oxygen in fcc and hcp sites.

Upon on-surface oxygen adsorption, the Pb atoms on the three outmost layers exhibit lateral and vertical displacements, which are plotted in Fig. 6 for energetically stable fcc adsorption at different coverage. From the left panel (atomic

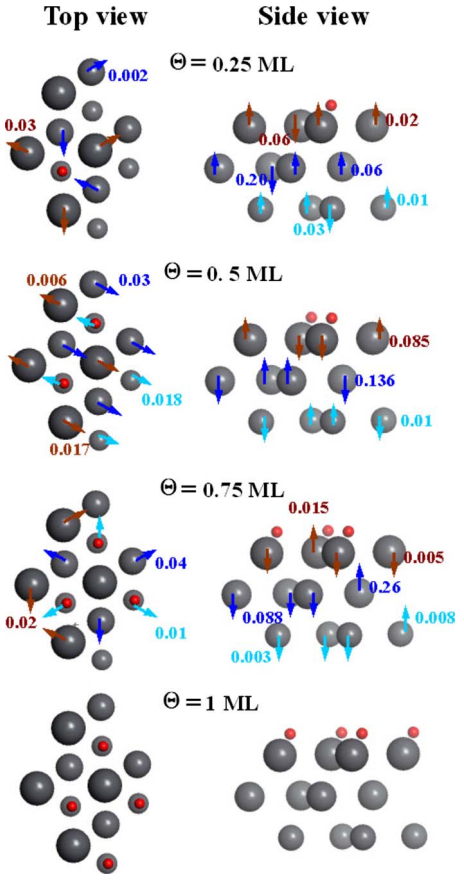

FIG. 6. (Color online) Different structures of oxygen adsorbed in the fcc site on Pb(111) surface. The left part shows the top view of the three outmost Pb layers. The right-hand part shows a side view of the vertical positions of the ions, cut in the plane along the $[1\bar{2}1]$ direction. Note, the gray balls with different scales represent Pb atoms on the different layers (the larger ball is the outer), and the small red balls represent the oxygen atoms. The arrows (not to scale) indicate the directions of the atomic displacements, with different colors standing for different layers. The numbers that refer to the arrows are given in angstrom.

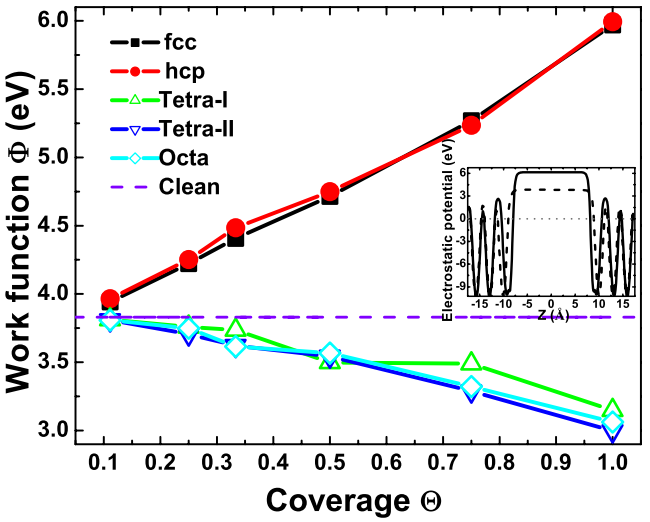

FIG. 7. (Color online) The calculated work function Φ as a function of Θ for different on-surface and subsurface adsorption sites. The dashed line shows the value of Φ for clean Pb(111) substrate. As an example, the inset shows the planar-averaged electrostatic potential of clean (dashed curve) and O-adsorbed (solid curve with Θ=1.0) Pb(111) slab, with the Fermi energies for both cases set at zero.

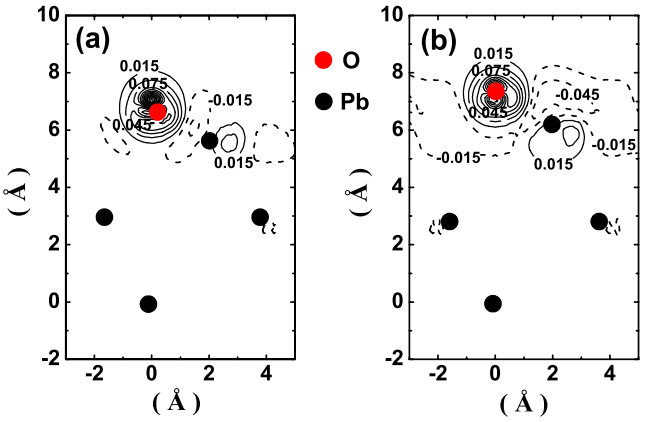

FIG. 8. (Color online) Contour plot of the charge density difference $\Delta n(\mathbf{r})$ for the on-surface O/Pb(111) slab with oxygen coverage (a) Θ=0.25 and (b) Θ=1.0. Solid and dashed lines denote increased and decreased electron density, respectively. The contour plane is parallel with the $[1\bar{2}1]$ direction and is perpendicular to the Pb(111) surface.

top view) of Fig. 6, one can see that Pb atoms bonded to oxygen in top layer always move outwards from chemisorbed oxygen for different coverage with the same surface model. The values of atomic movements are also indicated in the figure. The right panel (side view) of Fig. 6 depicts the vertical movement of Pb atoms from the center of mass of each layer. One prominent feature is that the oxygen at various coverage (except for the case Θ=1.0) we considered causes a most noticeable rumpling of the second Pb layer, which can be seen by large value of vertical movement of the second Pb layer.

We turn now to analyze the electronic properties of the O/Pb(111) system by first considering the work function Φ, which is plotted in Fig. 7 and summarized in Table II for different oxygen coverage. From Fig. 7, it can be seen that the work function steadily increases with O coverage for both fcc and hcp on-surface adsorption. Comparing to the other TM surfaces such as Ag(111), we notice that the varying amplitude of Φ in the whole coverage at the present Pb(111) surface is much smaller. In fact, from Fig. 7 one can see that the change of Φ with respect to the clean Pb(111) surface varies from ~0.4 eV at Θ=0.25 to ~2.1 eV at Θ=1.0 for both fcc and hcp on-surface adsorption, much smaller than in O/Ag(111) system (from ~1.2 eV at Θ=0.25 to ~4.0 eV at Θ=1.0).[20] On the other hand, our results of Φ versus Θ can be comparable with those for the other O-adsorbed *sp* simple metal surfaces such as Al(111) (Ref. 47) and Mg(0001).[51] Also from Fig. 7 it can be seen that the work functions are almost identical for the hcp and fcc adsorption configurations.

To gain more insight into the nature of Pb-O chemical bonding during oxygen adsorption onto the Pb(111) surface, we now analyze our results by means of the electron density difference $\Delta n(\mathbf{r})$, which is obtained by subtracting the electron densities of noninteracting component systems, $n^{\mathrm{Pb(111)}}(\mathbf{r})+n^{\mathrm{O}}(\mathbf{r})$, from the density $n(\mathbf{r})$ of the O/Pb(111) system, while retaining the atomic positions of the component systems at the same location as in O/Pb(111). Figures 8(a) and 8(b) present the contour plots of $\Delta n(\mathbf{r})$ for Θ=0.25 and Θ=1.0, respectively. One can see that the charge redistribution mainly occurs at the surface and involves the O adatom and the topmost Pb atoms. It is apparent that upon adsorption, electrons flow from Pb 6*p* into O 2*p* orbitals, resulting in a depletion of the surface metallic electrons. With the increase in oxygen coverage, it shows in Fig. 8 that more Pb 6*p* electrons transfer to the localized O 2*p* orbitals, which implies that the ionicity of the Pb-O bonding increases with oxygen coverage. On the other hand, there is also an important covalent component in Pb-O chemical bonding (see Fig. 9 below for details). The unique signature of this covalency occurred in Fig. 8 is the emergence of Pb $6s^2$ sterically active "lone pair," which, due to the hybridization with O 2*p* states, forms an enhanced density on the side of the Pb atom that points away from the PbO layers. The degree of this Pb(6*s*)-O(2*p*) hybridization increases with oxygen coverage, which is clearly shown in Fig. 8(b) by more electron accumulation in the mutual spatial region of Pb 6*s* and O 2*p* orbitals at Θ=1.0. Prominently, the enhanced Pb(6*s*)-O(2*p*) covalent interaction with oxygen coverage reflects the decreased (increased) covalent (ionic) interaction between surface Pb 6*p* and O 2*p* atomic orbitals. For pure PbO crystal in α or β phase, recent theoretical[61] and experimental[69] studies have shown that the Pb $6s^2$ lone pair is a result of the lead-oxygen interaction. Our present finding shows that this lone pair also occurs during Pb(111) surface oxidation process and may play a fundamental role in determining the oxygen binding energy and large interlayer relaxation upon adsorption. Another fact shown in Fig. 8 is that similar to other oxygen/metal systems, the influence of the adsorbed Pb(111) surface is rapidly screened out on going into the bulk. The bonding character of the inner Pb layers (from the second layer for Θ=0.25 and from the third layer for Θ=1.0) is

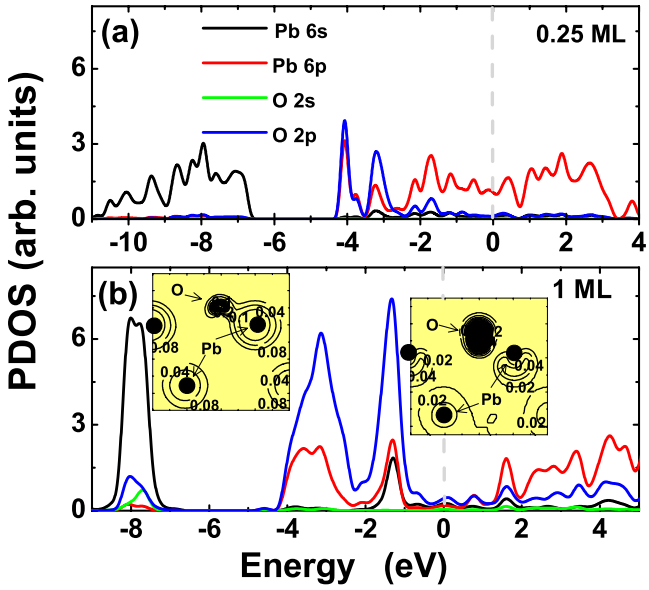

FIG. 9. (Color online) Orbital-resolved partial DOS for the surface Pb layer and the on-surface O adatom (fcc site) with the coverage (a) $\Theta=0.25$ and (b) $\Theta=1.0$. The left-side inset in (b) depicts the band charge density around $E=-8$ eV, while the right-side inset plots the band charge density around $E=-1.7$ eV.

essentially identical to the bulk case, which is typically metallic with a fairly constant charge density between the atoms with slight directional bonding along the body diagonals. This can be clearly seen in Fig. 8 by negligibly small changes in the interior of the ten-layer Pb slab at both low ($\Theta=0.25$) and high ($\Theta=1.0$) coverage. The charge accumulation on the surface and charge depletion below the surface will result in the formation of a dipole moment (in line with the usual surface dipole layer), which tends to increase the work function as discussed above.

Figures 9(a) and 9(b) show the orbital-resolved PDOS for the on-surface O_{fcc} layer and the topmost Pb layer at $\Theta=0.25$ and $\Theta=1.0$, respectively. At low coverage ($\Theta=0.25$), the left-side peak of O $2p$ [around −4.0 eV in Fig. 9(a)] represents the degenerate $2p_x$ and $2p_y$ states, which hybridize with the degenerate $6p_{x,y}$ states of the outmost Pb atoms. Whereas, the right-side peak of O $2p$ [around −3.2 eV in Fig. 9(a)] represents the mixed $2p_{x,y}$ and $2p_z$ states (with the latter a little lower in energy than the former), which hybridize with the Pb $6p_{x,y}$ and $6p_z$ states. One can see that the coupling between Pb $6s$ and O $2p$ states is negligibly small at low coverage, which implies that the lone pair effect of Pb $6s^2$ is small at low coverage. In addition, it also shows in Fig. 9(a) that on the whole, the metallic nature of surface Pb(111) layer does not change by low coverage of oxygen. This feature can be seen by the fact that the PDOS at E_F for the topmost Pb layer is comparable with that for clean Pb(111) surface. With increasing oxygen coverage [Fig. 9(b) for $\Theta=1.0$], four prominent changes involving the O-Pb chemical bonding occur: (i) the DOS for the surface Pb atoms is significantly suppressed at the Fermi level (see Fig. 10 for more clear illustration); (ii) The energy distribution around $E=-8.0$ eV for the surface-layer Pb $6s$ state becomes very narrow compared to the cases of clean and low-coverage surfaces. Actually, from the band charge density around $E=-8.0$ eV, as plotted in the left-side inset in Fig. 9(b), it can be seen that at this energy interval, the surface Pb atoms have more and dense charge compared to the second-layer Pb atoms; (iii) The hybridization of O $2p$ and Pb $6s$ states near the top of the valence band is distinctly enhanced, which means that the high oxygen coverage favors the formation of Pb $6s^2$ lone pair. To see this better, we plot in the right-side inset in Fig. 9(b) the band charge around $E=-1.7$ eV, which clearly displays a distorted $6s$ charge distribution around the surface Pb atom. More interestingly, at high oxygen coverage, there also appears an increasing hybridization between O $2p$ and Pb $6s$ states around $E=-8.0$ eV, which further supports the physical picture of Pb $6s^2$ lone pair; (iv) The energy distance between the two O $2p$ (or their hybridized Pb $6p$) peaks increases from 0.8 eV at $\Theta=0.25$ to 2.0 eV at $\Theta=1.0$. To further illustrate the incremental influence of oxygen coverage on the surface chemical bonding, we plot in Fig. 10 the total DOS of the O_{fcc} and topmost Pb atoms for different coverage calculated from the $p(2\times2)$ surface model. One can see that the density at the Fermi energy monotonically decreases with increasing the coverage, and the metallic $6p$ bands of the topmost Pb layer gradually evolve into the insulating bands due to their ionic as well as covalent coupling with O $2p$ orbitals. Therefore, Fig. 10 clearly shows the tendency to the formation of an insulating surface by the increase in oxygen coverage. This insulating surface has been effectively used to control the many-body interaction between the magnetic molecule and the Pb(111) surface in recent experiment.[70]

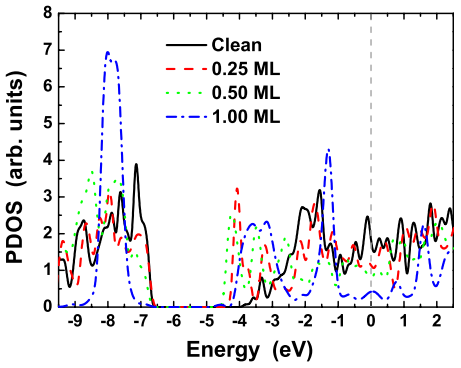

FIG. 10. (Color online) Total DOS of the on-surface O adatoms (fcc site) and the surface-layer Pb atoms for different values of the coverage Θ.

V. PURE SUBSURFACE ADSORPTION

In parallel with Sec. IV, in this section we continue to study the subsurface adsorption of atomic oxygen without the presence of on-surface oxygen, namely, pure subsurface adsorption. For oxygen occupation in subsurface region there are three different high-symmetry sites. The octahedral site (henceforth octa) lies just underneath the on-surface fcc site, and one tetrahedral site (tetra-I) lies below the on-surface hcp site. A second tetrahedral site (tetra-II) is located directly below a first-layer metal atom. The coordinates of these sub-

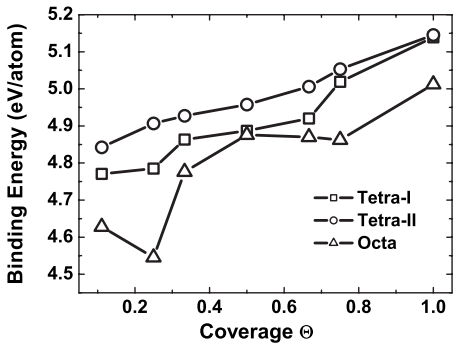

FIG. 11. Binding energies E_b for oxygen in the subsurface tetra-I, tetra-II, and octa adsorption sites as functions of the O coverage.

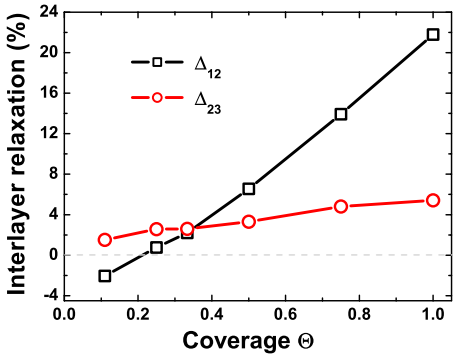

FIG. 12. (Color online) Interlayer relaxations as functions of coverage for oxygen in subsurface tetra-II site.

surface sites were schematically shown in Fig. 1. We performed calculations for oxygen in these different sites in a wide range of coverage, i.e., from 0.11 to 1.0 ML. Note that we focus on adsorption immediately below the first Pb layer as we find that oxygen adsorption deep in the bulk is less favorable in every case. The case of simultaneous subsurface and on-surface oxygen adsorption will be studied in a forthcoming paper. In the following, the energetics, the atomic structure, and the electronic properties for the subsurface adsorption are discussed in detail.

The calculated binding energies E_b for $O_{tetra\text{-}I}$, $O_{tetra\text{-}II}$, and O_{octa}, with respect to a free oxygen atom, are plotted in Fig. 11 and summarized in Table II. One can see that the most preferred adsorption site is tetra-II site for the whole coverage range and among all the on-surface and subsurface adsorption sites considered. This is remarkably different from the other systems such as O/Ag(111), O/Cu(111), and O/Mg(0001). For $O_{tetra\text{-}II}$ (open circles in Fig. 11) or $O_{tetra\text{-}I}$ (open squares), the binding energy increases slightly but steadily with O coverage, which is similar to the case of on-surface adsorption. For O_{octa} adsorption (open triangles), the binding energy decreases when the coverage Θ varies from 0.11 to 0.25, indicating a repulsive interaction between the O_{octa} atoms; however, it increases again from $\Theta=0.33$ to 1.0, so that the effective interaction between the O_{octa} atoms is attractive in this coverage range. Despite these different dependence on coverage, we note that the overall variation in the magnitude of the binding energy as a function of Θ is rather small for the three subsurface sites, namely, 0.33 eV, 0.51 eV, and 0.50 eV for $O_{tetra\text{-}II}$, $O_{tetra\text{-}I}$, and O_{octa} atoms, respectively. Compared to the on-surface adsorption, the subsurface adsorption is notably more favorable in the whole range of coverage considered. In fact, the binding energy difference ΔE_b between the most energetically stable on-surface fcc and subsurface tetra-II adsorption increases from about 0.1 to 0.2 eV for the coverage from $\Theta=0.11$ to $\Theta=1.0$. The result that the subsurface adsorption is more stable than the on-surface adsorption has also been found in O/Mg(0001) system,[51] but with the different tendency with respect to oxygen coverage. In the O/Mg(0001) system it was found that the value of ΔE_b decreases from about 0.4 eV to less than 0.1 eV by increasing coverage Θ from 0.0625 to 1.0.[51]

Table IV presents the results for the O-Pb bond length R_1 and interlayer relaxations in a wide range of coverage for $O_{tetra\text{-}I}$, $O_{tetra\text{-}II}$, and O_{octa} adsorptions. For more clear illustration, the first (Δ_{12}) and second (Δ_{23}) interlayer relaxations with $O_{tetra\text{-}II}$ adsorption are also plotted in Fig. 12. One can see from Fig. 12 that the first interlayer relaxation Δ_{12} increases from −5% to about 22% as a function of Θ, while the second interlayer relaxation Δ_{23} is much insensitive to the variation of the coverage compared to Δ_{12}. From Table IV one can see that the value of R_1 for $O_{tetra\text{-}II}$ atoms keeps the most short and stable compared to the other on-surface or subsurface sites. Whereas, for the octa and tetra-I adsorption sites, it shows in Table IV that the amplitude of R_1 oscillates with oxygen coverage.

We turn now to study the electronic properties of the subsurface-adsorbed O/Pb(111) system by first considering

TABLE IV. The calculated interlayer relaxation Δ_{ij} (%) and O-Pb bond length R_1 (in Å) for different oxygen coverage of subsurface adsorption.

Coverage	R_1 (Å)			Δ_{12} (%)			Δ_{23} (%)		
Θ	tetra-I	tetra-II	octa	tetra-I	tetra-II	octa	tetra-I	tetra-II	octa
0.11	2.342	2.255	2.452	−3.238	−2.058	−3.065	2.875	1.516	1.703
0.25	2.288	2.268	2.379	0.129	0.757	0.037	3.773	2.577	0.436
0.33	2.346	2.265	2.497	−1.405	2.205	0.373	6.139	2.607	1.840
0.50	2.304	2.265	2.380	12.22	6.547	13.77	3.190	3.301	2.557
0.75	2.312	2.265	2.270	15.16	13.92	13.55	6.022	4.809	−1.861
1.00	2.351	2.254	2.327	25.18	21.80	22.25	1.407	5.420	−3.988

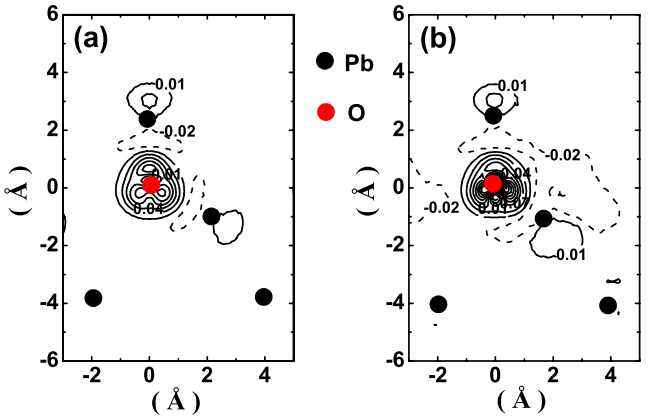

FIG. 13. (Color online) Contour plots of the charge density difference $\Delta n(\mathbf{r})$ for the subsurface $O_{tetra\text{-}II}$/Pb (111) slab with oxygen coverage (a) $\Theta=0.25$ and (b) $\Theta=1.0$. Solid and dashed lines denote increased and decreased electron density, respectively. The contour plane is parallel with the $[1\bar{2}1]$ direction and is perpendicular to the Pb(111) surface.

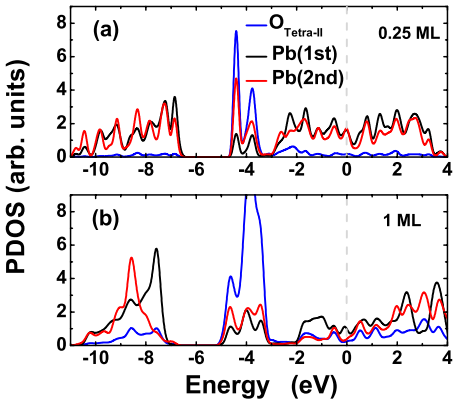

FIG. 14. (Color online) Layer-projected DOS for the $O_{tetra\text{-}II}$ subsurface layer and the outmost two Pb(111) layers.

the work function Φ and its change $\Delta\Phi$ with respect to the clean Pb(111) surface, both of which are illustrated in Fig. 7 and summarized in Table II at different oxygen coverage. It can be seen that the work function slightly but steadily decreases with coverage for subsurface adsorption. The overall variation in the magnitude of the work-function change $\Delta\Phi$ is rather small, namely, −0.8 eV, −0.66 eV, and −0.73 eV for $O_{tetra\text{-}II}$, $O_{tetra\text{-}I}$, and O_{octa}, respectively. These results of $\Delta\Phi$ versus Θ are comparable to those in O/Al(111) system,[47] in which relatively small work-function change was observed despite the strong electron transfer between adsorbate and Al atoms, and was associated with the small adsorption distance for the O species.[71]

To gain more insight into the nature of the O subsurface adsorption, we now analyze our results by means of the charge density difference $\Delta n(\mathbf{r})$. Figures 13(a) and 13(b) present the contour plots of $\Delta n(\mathbf{r})$ for $\Theta=0.25$ and $\Theta=1.0$, respectively, for tetra-II subsurface adsorption. It reveals that the charge redistribution mainly involves the subsurface O and the two outmost Pb layers. The electrons flow upon adsorption from the first- and second-layer Pb atoms to O $2p$ orbitals. It is apparent that the adsorbed O $2p$ orbitals are not the same as those of the free O atom but they are polarized along the three Pb-O axis. This polarization is reasonable because the Pb atoms are positively charged. The subsurface accumulation and the on-surface depletion in the charge density would result in the formation of a dipole moment (antiparalleling with the usual surface dipole layer), which tends to reduce the work function as compared to that for the clean Pb(111) surface, as shown in Fig. 7. Also one can see from Fig. 13 that the bonding character of the inner Pb layers (from the third layer) is essentially identical to the bulk case, while the first- and second-layer Pb atoms show remarkable changes in the charge density, reflecting the strong influence of the neighboring subsurface O atom. As with the on-surface adsorption, both ionic and covalent components exist in the oxygen/Pb chemical bonding. The ionicity is reflected by charge transfer and polarization, while the covalency can be clearly seen from Fig. 13 by the occurrence of Pb $6s^2$ sterically active lone pairs, which point outward and inward the slab for the first- and second-layer Pb atoms, respectively.

Figures 14(a) and 14(b) show the PDOS for the subsurface $O_{tetra\text{-}II}$ layer and the first and second Pb(111) layers at $\Theta=0.25$ and $\Theta=1.0$, respectively. At low coverage ($\Theta=0.25$), O $2p$ states mainly hybridize with Pb $6p$ states, while the interaction between O $2p$ states and Pb $6s$ states is negligibly small. Note that O $2p$ states couple to $6p$ states of the second Pb layer more strongly than those of the first Pb layer, since the two peaks around −4 eV (below the Fermi energy) in Fig. 14(a) mainly consist of $2p$ states of $O_{tetra\text{-}II}$ atoms and $6p$ states of the second Pb layer, while the contribution from the first-layer Pb atoms is small. The reason is simply that the $6p$ states for the outmost Pb layer approach more close to the Fermi energy due to the metallic nature of the outmost Pb layer at low coverage. At as high coverage as $\Theta=1.0$ [Fig. 14(b)], two prominent new features occur. First, the PDOS shifts downward in energy and a large spectra weight near the Fermi energy (from below) becomes very small. This obviously will lead to the increase in the adsorption energy. Second, the coupling between O $2p$ and Pb $6s$ states comes to play an important role as a result of the Pb $6s$ lone pair effect as discussed above. Remarkably, the difference in the orientation of the $6s^2$ lone pair between the first- and second-layer Pb atoms gives rise to a weight splitting in the $6s$ PDOS of the two Pb layers, as shown in Fig. 14(b). In addition, compared to the high-coverage on-surface adsorption [Fig. 9(b)], the narrowing effect of Pb $6s$ states due to its coupling with O $2p$ states is less distinct.

VI. ENERGY BARRIER FOR ATOMIC OXYGEN DIFFUSION

Diffusion of atomic oxygen after on-surface dissociation of O_2 is an elementary process during the whole surface oxidation process, which is still in debate for many systems regarding the existence of "hot" atoms with transient mobility upon O_2 dissociation.[72–74] Also, the oxygen diffusion plays a key role in understanding many important catalytic reactions, such as oxidation of CO and hydrocarbons in the

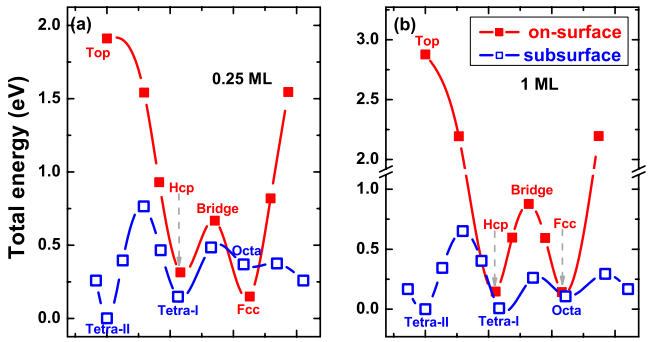

FIG. 15. (Color online) Total energy for an oxygen atom carrying out the on-surface (filled squares) or the subsurface (open squares) diffusion on Pb(111) face at the O coverage of (a) $\Theta=0.25$ and (b) $\Theta=1.0$. Here the total energy is given in reference to the most stable subsurface tetra-II occupation.

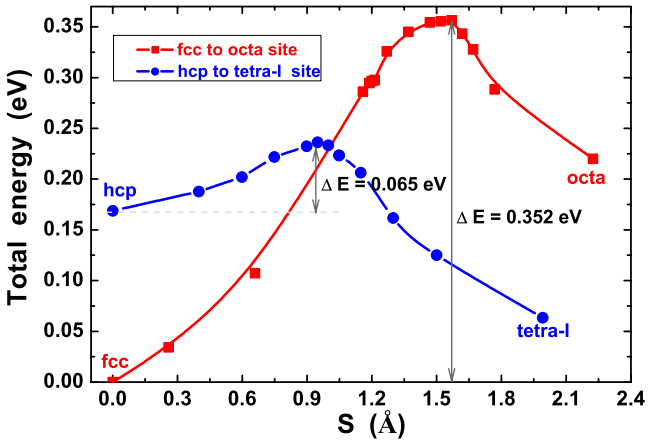

FIG. 16. (Color online) Total energy for an oxygen atom carrying out the penetration from the on-surface fcc to the subsurface octa site (filled squares) or from the on-surface hcp to the subsurface tetra-I site (filled circles) of Pb(111) lattice. Here the O coverage is set $\Theta=0.25$ and the total energy is given in reference to the on-surface fcc occupation. *s* coordinate indicates the penetration distance of the O atom with respect to the initial on-surface fcc or hcp adsorption site.

catalytic treatment of the automotive exhaust gases. In this section, by using the DFT total energy calculation, we report our numerical results of the energy barriers for atomic O diffusion and penetration in the O/Pb(111) system.

Using the nudged elastic band (NEB) method,[75–77] which is capable of finding saddle points and minimum energy paths on complicated potential surfaces, we have calculated the on-surface and subsurface diffusion-path energetics of atomic oxygen. The results are shown in Fig. 15(a) for low ($\Theta=0.25$) coverage and in Fig. 15(b) for high ($\Theta=1.0$) coverage. Note that in each figure [Fig. 15(a) and 15(b)] the number of atoms keeps invariant in the on-surface and subsurface calculations. Thus it also reveals in Fig. 15 the relative stability of O adsorption among various on-surface and subsurface sites and the corresponding oxygen binding energy differences. For the on-surface adsorption, our calculated diffusion barrier from fcc to hcp site is 0.52 eV at $\Theta=0.25$ and 0.74 eV at $\Theta=1.0$. The hcp site is less stable than the fcc site within the coverage $0<\Theta\leq 1$, although the binding energy difference between O_{fcc} and O_{hcp} decreases rapidly when increasing Θ (see Fig. 3). Thus the on-surface diffusion barrier from hcp to fcc site presents an activation barrier with the value of 0.35 eV at $\Theta=0.25$ and 0.73 eV at $\Theta=1.0$. For the subsurface adsorption, Fig. 15 shows that all of the three sites we considered, i.e., the tetra-I, the tetra-II, and the octa sites, present the local energy minimum along the oxygen subsurface diffusion path. The subsurface diffusion barrier from tetra-II to tetra-I site is 0.76 eV at $\Theta=0.25$ and 0.64 eV at $\Theta=1.0$. For the diffusion from tetra-I to octa site, the calculated energy barrier is 0.28 eV at $\Theta=0.25$ and 0.25 eV at $\Theta=1.0$. For the diffusion from tetra-II to octa site, the calculated barrier is 0.37 eV at $\Theta=0.25$ and 0.29 eV at $\Theta=1.0$. The octa site is less stable than the tetra-I site, while the tetra-I site is less stable than the tetra-II site. Thus the subsurface diffusion barrier from tetra-I to tetra-II site presents an activation barrier with the value of 0.62 eV at $\Theta=0.25$ and 0.64 eV at $\Theta=1.0$. In the same way, the activation barrier for octa$\rightarrow$tetra-I diffusion is 0.11 eV at $\Theta=0.25$ and 0.16 eV at $\Theta=1.0$, while the activation barrier for octa$\rightarrow$tetra-II diffusion is 0.01 eV at $\Theta=0.25$ and 0.18 eV at $\Theta=1.0$.

To investigate subsurface oxygen in more detail with regard to the energetics of its formation, we now study the penetration process of oxygen atom. Note that although the subsurface tetra-II site is most stable, the direct oxygen penetration into this site from the on-surface adsorption without bypassing the other subsurface sites is very unfavorable, since this site is located beneath a surface Pb atom. Therefore, here we only consider the penetration of an oxygen atom from the on-surface fcc (hcp) to the neighboring subsurface octa (tetra-I) site at the coverage $\Theta=0.25$. For this purpose, we fully relax the first three Pb layers, and restrain the oxygen atom when approaching to the first Pb layer step by step to search for the transition state with high energy. The calculated penetration paths and the energy barriers from the on-surface fcc to subsurface octa site and from the on-surface hcp to subsurface tetra-I site are shown in Fig. 16, in which the *s* coordinate indicates the penetration distance of the O atom with respect to the initial on-surface fcc or hcp adsorption site. The calculated penetration barrier from on-surface fcc to subsurface octa site is 0.352 eV. The transition state, i.e., the atomic geometry of the energy maximum in the penetration path, corresponds to the oxygen atom 0.1 Å above the surface Pb layer. For penetration from the on-surface hcp to the subsurface tetra-I site, the calculated activation barrier is as small as 0.065 eV, which implies the most favorable path for the oxygen penetration. The transition state corresponds to the oxygen atom 0.4 Å below the surface Pb layer. Comparing to the energy barriers for the O on-surface diffusion, one can see that the oxygen atoms can easily intrude into the subsurface and bond with the second-layer Pb atoms rather than searching for a more stable on-surface site (fcc site) to settle down. Even though an oxygen atom settles down at the stable on-surface fcc site, it also can penetrate into the subsurface stimulated by a slight perturbation.

VII. CONCLUSIONS

In summary, we have systematically investigated the adsorption of atomic oxygen on the Pb(111) surface and sub-

surface, as well as the energy barriers for atomic O diffusion and penetration in these systems through first-principles DFT-GGA calculations. We have considered a wide range of coverage using different surface models [i.e., $p(3\times3)$, $p(2\times2)$, $p(\sqrt{3}\times\sqrt{3})$, and $p(1\times1)$ surface unit cells] for adsorption in the on-surface fcc and hcp sites, as well as in the subsurface tetra-I, tetra-II, and octa sites. For the on-surface adsorption, the fcc site is more stable than the hcp site for the whole coverage range considered. The difference of the oxygen binding energies between these two sites decreases with increasing coverage. In particular, at the coverage of 1 ML, the binding energy of O_{hcp} is almost equal to that of O_{fcc}, implying a critical coverage for the stability conversion between the on-surface fcc and hcp sites. The atomic geometry, the work-function change, the charge density distribution, and the electronic structure upon the O on-surface adsorption have also been studied, which consistently show the fundamental influence by the ionic as well as covalent bonding between the O adatom and the first-layer Pb atoms. Remarkably, this influence in the energetics and atomic structure is monotonically enhanced with increasing the O coverage, which is highly interesting. For instance, the increase in the O binding energy for the fcc or the hcp site with increasing the coverage implies the effective attraction between the O adsorbates, which will make it favorable for the formation of the oxygen island or cluster. Furthermore, we have found that with increasing oxygen coverage, the surface Pb $6s^2$ lone pair effect becomes prominent. Also, the surface electronic DOS at the Fermi energy rapidly decreases with oxygen coverage, which will further stabilize the system in accordance with the increase in binding energy.

For the subsurface adsorption, we have shown that the tetra-II site is more stable than the tetra-I and octa sites. A similar correlation between the binding energy and the coverage has been found for $O_{tetra\text{-}I}$ and $O_{tetra\text{-}II}$, which also implies the effective attraction between the adsorbed O atoms and the tendency to form oxygen island or cluster at subsurface sites. The other atomic and electronic structural properties of the subsurface adsorption have also been investigated. The observed increase in the first-second Pb interlayer expansion, the decrease in the work-function change $\Delta\Phi$, and the decrease in the PDOS at the Fermi energy as functions of the O coverage consistently show the stabilization of the O-Pb chemical bonding, which is featured by the charge transfer from the first- and second-layer Pb atoms to the subsurface O atom, as well as by the formation of the Pb $6s^2$ lone pair.

Given the observation that the oxygen subsurface adsorption is more stable than the on-surface adsorption, we have then calculated the on-surface and subsurface diffusion-path energetics of atomic oxygen. The activation barrier for the on-surface or the subsurface O diffusion becomes high when increasing the coverage, which indicates the competition between the attractive interaction from the adsorbate and the substrate and the repulsive force among the adsorbates. In particular, we have shown that the activation barrier for the penetration from the on-surface hcp to the subsurface tetra-I site is as low as 0.065 eV, which indicates that the oxygen atoms can directly incorporate into the lead (below the topmost Pb layer) right after on-surface O_2 dissociation at low coverage.

ACKNOWLEDGMENTS

This work was supported by the NSFC under Grants No. 10604010 and No. 60776063. One of the authors (B.S.) is grateful for fruitful discussions with X.-L. Chen.

*Corresponding author; zhang_ping@iapcm.ac.cn

[1] K. Thürmer, E. Williams, and J. Reutt-Robey, Science **297**, 2033 (2002).
[2] P. Jiang, X. Ma, L. L. Wang, Y. S. Fu, S. H. Ji, Y. Qi, J. Jia, and Q.-K. Xue (unpublished).
[3] X. Ma, P. Jiang, Y. Qi, J. Jia, Y. Yang, W. Duan, W.-X. Li, X. Bao, S. B. Zhang, and Q.-K. Xue, Proc. Natl. Acad. Sci. U.S.A. **104**, 9204 (2007).
[4] P. Jiang, X. Ma, Y. Yang, Y. X. Ning, L. L. Wang, Y. S. Fu, S. H. Ji, Y. Qi, W. Duan, S. B. Zhang, J. Jia, and Q.-K. Xue (unpublished).
[5] M. Alatalo, S. Jaatinen, P. Salo, and K. Laasonen, Phys. Rev. B **70**, 245417 (2004), and references therein.
[6] S. Jaatinen, J. Blomqvist, P. Salo, A. Puisto, M. Alatalo, M. Hirsimäki, M. Ahonen, and M. Valden, Phys. Rev. B **75**, 075402 (2007).
[7] J. C. Yang, B. Kolasa, J. M. Gibson, and M. Yeadon, Appl. Phys. Lett. **73**, 2841 (1998).
[8] Y. Xu and M. Mavrikakis, Surf. Sci. **494**, 131 (2001).
[9] A. Soon, M. Todorova, B. Delley, and C. Stamplf, Phys. Rev. B **73**, 165424 (2006).
[10] G. Ertl, Surf. Sci. **6**, 208 (1967).
[11] J. Haase and H. J. Kuhr, Surf. Sci. **203**, L695 (1988).
[12] F. Jensen, F. Besenbacher, E. Lægsgaard, and I. Stensgaard, Surf. Sci. **259**, L774 (1991).
[13] S. M. Johnston, A. Mulligan, V. Dhanak, and M. Kadodwala, Surf. Sci. **519**, 57 (2002).
[14] M. Rocca, L. Savio, L. Vattuone, U. Burghaus, V. Palomba, N. Novelli, F. Buatier de Mongeot, U. Valbusa, R. Gunnella, G. Comelli, A. Baraldi, S. Lizzit, and G. Paolucci, Phys. Rev. B **61**, 213 (2000).
[15] L. Savio, L. Vattuone, M. Rocca, F. Buatier de Mongeot, G. Comelli, A. Baraldi, S. Lizzit, and G. Paolucci, Surf. Sci. **506**, 213 (2002).
[16] M. A. Barteau and R. J. Madix, J. Electron Spectrosc. Relat. Phenom. **31**, 101 (1983).
[17] C. T. Campbell and M. T. Paffett, Surf. Sci. **143**, 517 (1984).
[18] V. I. Bukhtiyarov, V. V. Kaichev, and I. P. Prosvirin, J. Chem. Phys. **111**, 2169 (1999).
[19] C. T. Cambell, Surf. Sci. **173**, L641 (1986), and references therein.
[20] W.-X. Li, C. Stampfl, and M. Scheffler, Phys. Rev. B **65**, 075407 (2002).
[21] W.-X. Li, C. Stampfl, and M. Scheffler, Phys. Rev. B **67**, 045408 (2003).
[22] M.-L. Bocquet, A. Michaelides, P. Sautet, and D. A. King, Phys.

Rev. B **68**, 075413 (2003).
[23] G. Rovida, F. Pratesi, M. Maglietta, and E. Ferroni, Surf. Sci. **43**, 230 (1974).
[24] C. T. Campbell, Surf. Sci. **157**, 43 (1985).
[25] C. I. Carlisle, D. A. King, M. L. Bocquet, J. Cerdá, and P. Sautet, Phys. Rev. Lett. **84**, 3899 (2000).
[26] M. V. Ganduglia-Pirovano and M. Scheffler, Phys. Rev. B **59**, 15533 (1999).
[27] M. V. Ganduglia-Pirovano, K. Reuter, and M. Scheffler, Phys. Rev. B **65**, 245426 (2002).
[28] G. Comelli, V. R. Dhanak, M. Kiskinova, K. C. Prince, and R. Rosei, Surf. Sci. Rep. **32**, 165 (1998), and references therein.
[29] J. Wider, T. Greber, E. Wetli, T. J. Kreutz, P. Schwaller, and J. Osterwalder, Surf. Sci. **417**, 301 (1998); **432**, 170 (1999).
[30] E. Lundgren, G. Kresse, C. Klein, M. Borg, J. N. Andersen, M. De Santis, Y. Gauthier, C. Konvicka, M. Schmid, and P. Varga, Phys. Rev. Lett. **88**, 246103 (2002), and references therein.
[31] G. Zheng and E. I. Altman, Surf. Sci. **462**, 151 (2000).
[32] A. P. Seitsonen, Y. D. Kim, S. Schwegmann, and H. Over, Surf. Sci. **468**, 176 (2000).
[33] M. Todorova, K. Reuter, and M. Scheffler, J. Phys. Chem. B **108**, 14477 (2004).
[34] M. Todorova, K. Reuter, and M. Scheffler, Phys. Rev. B **71**, 195403 (2005).
[35] W.-X. Li, L. Österlund, E. K. Vestergaard, R. T. Vang, J. Matthiesen, T. M. Pedersen, E. Laegsgaard, B. Hammer, and F. Besenbacher, Phys. Rev. Lett. **93**, 146104 (2004).
[36] J. L. Gland, Surf. Sci. **93**, 487 (1980).
[37] A. Eichler and J. Hafner, Phys. Rev. Lett. **79**, 4481 (1997).
[38] A. Bogicevic, J. Strömquist, and B. I. Lundqvist, Phys. Rev. B **57**, R4289 (1998).
[39] H. Tang, A. Van der Ven, and B. L. Trout, Phys. Rev. B **70**, 045420 (2004).
[40] K. Reuter, M.-V. Ganduglia-Pirovano, C. Stampfl, and M. Scheffler, Phys. Rev. B **65**, 165403 (2002).
[41] C. Stampfl, S. Schwegmann, H. Over, M. Scheffler, and G. Ertl, Phys. Rev. Lett. **77**, 3371 (1996).
[42] K. Honkala and K. Laasonen, Phys. Rev. Lett. **84**, 705 (2000).
[43] T. Sasaki and T. Ohno, Phys. Rev. B **60**, 7824 (1999).
[44] L. C. Ciacchi and M. C. Payne, Phys. Rev. Lett. **92**, 176104 (2004).
[45] J. Behler, B. Delley, S. Lorenz, K. Reuter, and M. Scheffler, Phys. Rev. Lett. **94**, 036104 (2005).
[46] J. Jacobsen, B. Hammer, K. W. Jacobsen, and J. K. Nørskov, Phys. Rev. B **52**, 14954 (1995).
[47] A. Kiejna and B. I. Lundqvist, Phys. Rev. B **63**, 085405 (2001), and references therein.
[48] A. Kiejna, Phys. Rev. B **68**, 235405 (2003).
[49] A. Hellman, Phys. Rev. B **72**, 201403(R) (2005).
[50] E. Schröder, R. Fasel, and A. Kiejna, Phys. Rev. B **69**, 193405 (2004).
[51] E. Schröder, R. Fasel, and A. Kiejna, Phys. Rev. B **69**, 115431 (2004), and references therein.
[52] G. Kresse and J. Hafner, Phys. Rev. B **47**, 558 (1993); G. Kresse and J. Furthmüller, Comput. Mater. Sci. **6**, 15 (1996); G. Kresse and J. Furthmüller, Phys. Rev. B **54**, 11169 (1996).
[53] G. Kresse and D. Joubert, Phys. Rev. B **59**, 1758 (1999).
[54] M. Bockstedte, A. Kley, J. Neugebauer, and M. Scheffler, Comput. Phys. Commun. **107**, 187 (1997).
[55] *Princinciples of Surface Physics*, edited by F. Bechstedt (Springer-Verlag, Berlin, 2003).
[56] J. Neugebauer and M. Scheffler, Phys. Rev. B **46**, 16067 (1992).
[57] J. P. Perdew, J. A. Chevary, S. H. Vosko, K. A. Jackson, M. R. Pederson, D. J. Singh, and C. Fiolhais, Phys. Rev. B **46**, 6671 (1992).
[58] M. Weinert and J. W. Davenport, Phys. Rev. B **45**, 13709 (1992).
[59] H. J. Monkhorst and J. D. Pack, Phys. Rev. B **13**, 5188 (1976).
[60] C. Kittel, *Introduction to Solid State Physics*, 5th ed. (Wiley, New York, 1976).
[61] G. W. Watson, S. C. Parker, and G. Kresse, Phys. Rev. B **59**, 8481 (1999).
[62] D. J. Payne, R. G. Egdell, G. Paolicelli, F. Offi, G. Panaccione, P. Lacovig, G. Monaco, G. Vanko, A. Walsh, G. W. Watson, J. Guo, G. Beamson, P.-A. Glans, T. Learmonth, and K. E. Smith, Phys. Rev. B **75**, 153102 (2007).
[63] To test the Pb 5*d* electron effect, the O/Pb(111) system has been calculated by treating Pb 5*d* electrons as valence electrons at a 0.25 ML coverage. The Pb 5*d* states are found to be localized in the deep energy levels ranging from about −17 eV to −16 eV, with a weak hybridization with O 2*s* states. The calculated physical properties including the binding energy, work functuion, and interlayer relaxations show that the consideration of Pb 5*d* electrons (as valence electrons) does not change the preferred adsorption site for on-surface and subsurface adsorption. The binding energy has a very little increase of about 0.1 eV in quantity due to the consideration of Pb 5*d* electrons. But the work function, the Pb-O bonding length, and the interlayer relaxations are found to be quite similar to the results without considering the Pb 5*d* electrons.
[64] D. Yu and M. Scheffler, Phys. Rev. B **70**, 155417 (2004).
[65] Y. Jia, B. Wu, H. H. Weitering, and Z. Zhang, Phys. Rev. B **74**, 035433 (2006).
[66] A. Mans, J. H. Dil, A. R. H. F. Ettema, and H. H. Weitering, Phys. Rev. B **72**, 155442 (2005).
[67] H. Krakauer, M. Posternak, A. J. Freeman, and D. D. Koelling, Phys. Rev. B **23**, 3859 (1981).
[68] K. P. Huber and G. Herzberg, *Molecular Spectra and Molecular Structure IV: Constants of Diatomic Molecules* (Van Nostrand Reinhold, New York, 1979).
[69] D. J. Payne, R. G. Egdell, A. Walsh, G. W. Watson, J. Guo, P.-A. Glans, T. Learmonth, and K. E. Smith, Phys. Rev. Lett. **96**, 157403 (2006).
[70] Y.-S. Fu, S.-H. Ji, X. Chen, X.-C. Ma, R. Wu, C.-C. Wang, W.-H. Duan, X.-H. Qiu, B. Sun, P. Zhang, J.-F. Jia, and Q.-K. Xue, Phys. Rev. Lett. **99**, 256601 (2007).
[71] N. D. Lang, Surf. Sci. **127**, L118 (1983).
[72] J. Wintterlin, R. Schuster, and G. Ertl, Phys. Rev. Lett. **77**, 123 (1996).
[73] J. Harris and B. Kasemo, Surf. Sci. **105**, L281 (1981).
[74] H. Brune, J. Wintterlin, J. Trost, G. Ertl, J. Wiechers, and R. J. Behm, J. Chem. Phys. **99**, 2128 (1993).
[75] G. Mills and H. Jónsson, Phys. Rev. Lett. **72**, 1124 (1994).
[76] G. Mills, H. Jónsson, and G. Schenter, Surf. Sci. **324**, 305 (1995).
[77] M. Alatalo, S. Jaatinen, P. Salo, and K. Laasonen, Phys. Rev. B **70**, 245417 (2004).